



Subwavelength imaging in the visible range using metal coated carbon nanotube forest

Journal:	<i>Nanoscale</i>
Manuscript ID:	NR-ART-01-2014-000075.R1
Article Type:	Paper
Date Submitted by the Author:	25-Feb-2014
Complete List of Authors:	Choe, Jong-Ho; ETRI, Choi, Muhan; Kyungpook National University, School of Electronics Engineering Lee, Wonjun; KAIST, Kang, Byungsoo; Korea Advanced Institute of Science and Technology, Department of Mechanical Engineering Kim, Jinhung; Korea Advanced Institute of Science and Technology, Department of Physics Seo, Min-Kyo; Korea Advanced Institute of Science and Technology, Department of Physics Min, Bumki; Korea Advanced Institute of Science and Technology, Department of Mechanical Engineering Kim, Sang Ouk; KAIST, Materials Science and Engineering Choi, Choon-Gi; Electronics and Telecommunications Research Institute,

Cite this: DOI: 10.1039/c0xx00000x

www.rsc.org/xxxxxx

ARTICLE TYPE

Subwavelength imaging in the visible range using metal coated carbon nanotube forest

Jong-Ho Choe,^a Muhan Choi,^{ab} Won Jun Lee,^c Byungsoo Kang,^d Jinhyung Kim,^e Min-Kyo Seo,^e Bumki Min,^d Sang Ouk Kim,^c and Choon-Gi Choi^{*a}

⁵ Received (in XXX, XXX) Xth XXXXXXXXX 20XX, Accepted Xth XXXXXXXXX 20XX

DOI: 10.1039/b000000x

We demonstrate subwavelength imaging in the visible range by using a metal coated carbon nanotube forest. Under 532 nm illumination, a 160 nm separated double slit is resolved. This corresponds to the resolution of 0.3 wavelength. By control of the growing conditions and with the help of microtoming
10 technique, we made a dense carbon nanotube forest layer 400 nm thick. The metal coated carbon nanotube forest, acting as a wire medium nanolens, delivers the imaging information including details in the evanescent fields near the objects.

Introduction

Two point-like light sources are not resolved when their
15 separation is shorter than half the wavelength of the emitting light.¹ This is the well-known diffraction limit which arises from the fact that higher resolution information remains near the imaging object as evanescent fields, and does not propagate to the far distance. To overcome the diffraction limit, one should use
20 light whose wavelength is shorter than the size of the target to be resolved. This is the fundamental reason that human eyes cannot directly observe nano-sized structures even with the aid of delicate optics. In exploring the nano-world, electron
25 microscopes are usually adopted but they are not proper for fragile sample observations as in bio-applications and *in vivo* measurement. Due to the electron's high energy, the samples may suffer crucial damages during the measurement process. Therefore, it is important to develop a photonic based nano-
30 imaging system. Since the diffraction limit hinders imaging nano-structures, light sources below ultra-violet (UV) wavelengths are required. However, it is demanding to implement an imaging system using light sources below the UV wavelengths. Besides, with the decreasing wavelength, photon energy increases and this inevitably leads to the destruction of soft samples. These reasons
35 and the desire to directly see nano-structures provide the motivations for researchers to seek a way to overcome the diffraction limit.

To this end, various ideas have been suggested in the recent decade.²⁻⁵ One of the more widely known ideas was proposed by
40 Pendry, a 'perfect lens', which consists of negative refractive index material, and surpasses the diffraction limit by compensating decays of the evanescent field.⁶ However, negative refraction does not occur in natural bulk materials, so researchers have tried to realize negative refraction artificially using periodic
45 composite structures⁷⁻¹¹, and contemporarily, to develop another kind of superlens in which negative refraction is not

involved.¹²⁻¹⁶

These directions naturally led to investigations using a wired medium (periodic wire array) in imaging applications.³ Recently,
50 Kawata *et al.* proposed an optical imaging system using segmented silver nano-wires.¹⁷ Their nanolens can provide a magnified and colourful image of a nano-size object, in principle. Each nanowire in their nanolens works as a channel for an imaging pixel, so the resolution is determined by the separation
55 distances between wires in the bundle. Accordingly, to improve the resolving power of the endoscopic nanolens, making the wires small and in an appropriate arrangement are key points.

Experimentally, several endoscope-like imaging systems have been demonstrated in the microwave¹⁸ and infrared regions.¹⁹ To
60 realize a wire medium nanolens that works in the visible range, the diameter of the cylinder and the pitch of the cylinder array need to be much smaller than the wavelength of visible light. Furthermore, to support the plasmonic modes which carry imaging information of the object from the object interface to the
65 other interface of the nanolens, the cylinders in the wire medium should be metallic. One of the best candidate materials satisfying these conditions is the carbon nanotube (CNT).

In this article, we experimentally demonstrate a plasmonic subwavelength nano-imaging system that works in the visible
70 range by using a metal coated CNT forest nanolens. By controlling its growing conditions, the geometrical properties of the CNT structure, such as diameter, length and the pitch of the array, can be adjusted to be much smaller than the wavelength of visible light.

75 Fabrication and experiment

The fabrication process of the CNT forest is depicted schematically in Fig. 1(a), and the images of each step are presented in Fig. 1(b). To make the pitch of the CNT forest in a nanometer scale, we adopted a bottom-up fabrication technique
80 using a self-assembled block copolymer which is capable of

building up nano-structures within several tens of nanometer resolution.²⁰⁻²³ (see Supplement 1) Tilted evaporation of an iron layer over the block copolymer template can create nano-patterned iron catalysts (diameter ~ 9 nm) significantly smaller than the pore size of the block copolymer template (~ 43 nm). A subsequent heat treatment process reduces the size of the iron particles enough to form a single walled nanotubes array. The diameter, length, and the spacing between centers of nanotubes were 10-14 nm, ~ 30 μm , and 72 nm, respectively.

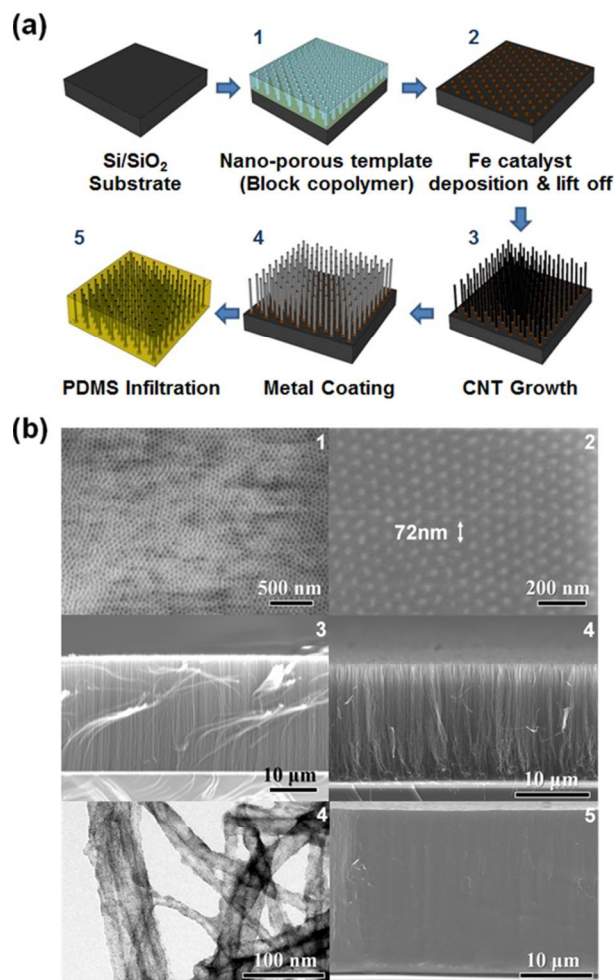


Fig. 1. (a) Schematic depiction of the hierarchical organization process used to fabricate metal coated vertical CNTs. (b) The SEM images of 1) nano-porous template, 2) patterned Fe catalyst, 3) as-grown CNTs, 4) Pt-coated CNTs and the TEM image of Pt-coated CNTs, 5) PDMS infiltrated CNTs. The images in (b) correspond to each process in the schematic (a) by numbering marks.

To support the plasmonic mode, we coated platinum on the CNT forest.²² The uniform coating of platinum particles was confirmed by transmission electron microscopy, depicted in Fig. 1(b). The reason we choose platinum instead of silver, which is a well-known plasmonic metal^{5,12}, is that silver forms aggregations when one tries to coat it on a CNT forest. After coating with platinum, polydimethylsiloxane (PDMS) polymer was infiltrated into the CNT forest for the purpose of fixing the CNT columns and sample transfer. Then, the CNT forest was peeled off and molded in ultratoming-purpose epoxy. We froze the CNT forest down to 77 K using liquid nitrogen and sliced it with a cryo-

ultratoming machine equipped with a precision diamond knife. Due to the low temperature environment, the PDMS was hardened enough to slice into 400 nm thick layers.

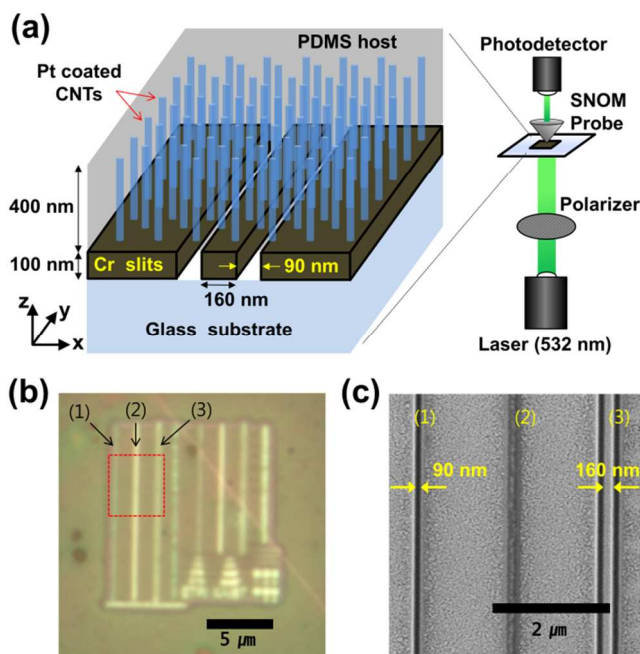


Fig. 2. (a) A schematic for the sample and the imaging experiment. CNTs are arranged in a hexagonal lattice with 80 nm pitch. A normal incident light of wavelength 532 nm, polarized perpendicular to slits, is illuminated. The light intensity distributed on the surface of the CNT forest nanolens is scanned by the SNOM imaging system. (b) A picture of the slit sample covered by the CNT forest nanolens. (c) The SEM image of the bare slit sample corresponds to the area in the red dashed box in (b). The numbering (1), (2), and (3) indicates a single slit, a less carved single slit and the 160 nm separated double slit, respectively.

The sliced metal coated CNTs, as a CNT forest nanolens, was placed on a double slit sample as depicted in Fig. 2(a). The double slit sample was prepared using focused ion beam (FIB, Quanta™ 3D FEG manufactured by FEI) to engrave a 100 nm thick chromium film on a glass substrate. The width of the slit was 90 nm and they were separated by 160 nm. The slits were entirely sandwiched by the CNT forest nanolens layer and the glass substrate. The optical image of the sample (CNT forest nanolens + slits + glass substrate) is shown in Fig. 2(b). The numbering (1), (2), and (3) in Fig. 2(b) indicates a single slit, a less carved single slit and the 160 nm separated double slit, respectively. The SEM image of the bare slit sample in Fig. 2(c) corresponds to the area inside the red dashed line in the Fig. 2(b).

The sample was placed in a scanning near-field optical microscope (SNOM, WITec Ins. Corp. alpha 300s) for near-field measurement. While scanning, the glass substrate was irradiated by diode laser ($\lambda_0 = 532$ nm) with polarization perpendicular to the slits. The near-field signals above the CNT forest nanolens were collected by the SNOM probe (aperture diameter: 60 nm) and entered to the photodetector.

Results and discussion

The SNOM measurement in Fig 3(a) shows a nanolens transferring an image of the light transmitted through the nano slit. As shown in the SEM image of the bare slits before attaching the

CNT forest nanolens layer, single and double slits are placed on the left and right, respectively. It is shown that 160 nm separated slits are clearly distinguished under 532 nm illumination. The separation is about one-third of the wavelength of incident light, so it is certain that the CNT forest nanolens works over the diffraction limit, transporting subwavelength scale images. During the SNOM scanning process, we changed the intensity of the laser for clear contrast electromagnetic field profile, so the image in Fig. 3(a) is striped and the SNOM signals are presented in various contrasts.

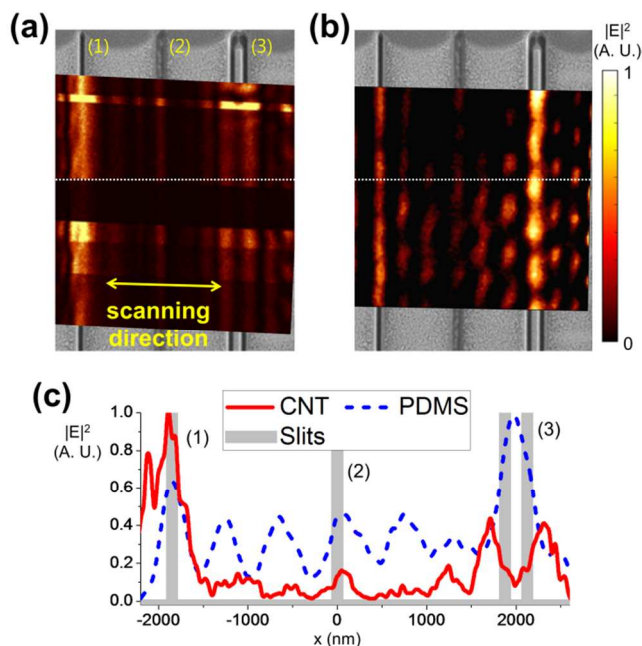
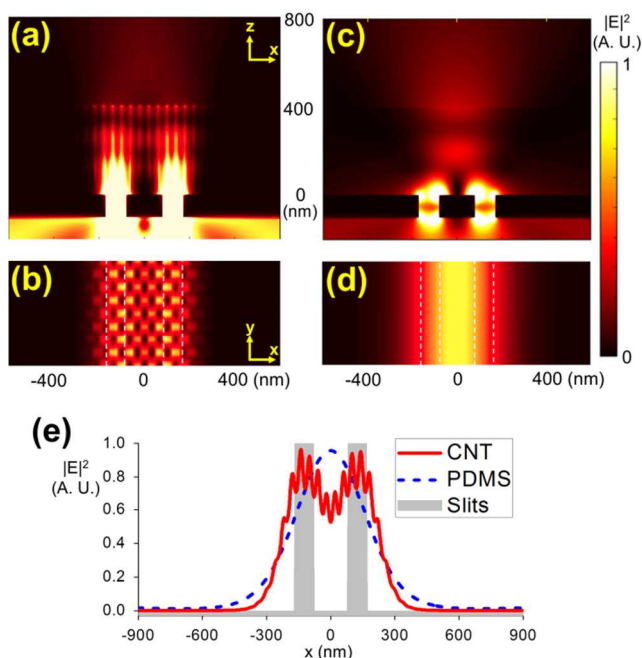


Fig. 3. (a) The SNOM image on CNT forest nanolens and SEM image of the slits are overlapped. The width of each slit is 90 nm. The double slit with 160 nm separation is resolved in various contrasts. (b) The SNOM image on PDMS coated slits and the SEM image of the slits are overlapped. As expected, the double slit is not resolved and the image is blurred because of the diffraction limit. (c) The cross cut of the field distributions are shown. The field intensity is presented in arbitrary units and the slit positions are indicated using grey bars.

To confirm whether the metal coated CNTs really transferred subwavelength scale imaging details from one side to the other, we performed contrast experiments without CNTs. In Fig. 3(b), the SNOM measurement image of a slit sample with just a PDMS coating is shown. In the sample, double and single slits are covered with a thin PDMS layer (about 410 nm, see Supplement 2). The electromagnetic field right after passing the slits should contain clearly distinguishable double slit image information. However as it passed through the PDMS layer, evanescent fields, which carry high spatial resolution information, decay from the slit apertures. Thus, as shown in the Fig 3(b) image, the electromagnetic fields reaching the other side of the PDMS layer lack subwavelength scale details, resulting in a blurred double slit image. Because of the diffraction limit, this result is expected, since the objective slits are separated by less than half the wavelength of the incident light. Figure 3(c) shows the cross cut of the field distributions along the white dotted line in Fig. 3(a) and (b). By comparing both cases in Fig. 3, it is certain that the CNTs bundle does have the ability to transport a subwavelength

scale image over distances.

For further support of our experiments, we also performed full 3D Finite-Difference Time-Domain (FDTD) calculations.²⁴ The FDTD results are presented in Fig. 4. In FDTD, we used platinum cylinders to simulate the platinum coated CNT forest. They were arranged in a hexagonal lattice of 80 nm pitch, immersed in a 400 nm thick PDMS with a refractive index of 1.4. Their diameter was 44 nm. The material dispersion was realized using the critical-point model,²⁵ applying permittivity parameters from other experimental references.²⁶ Just as in the experiment, the light was incident on chromium slits with polarization perpendicular to the slit direction.



The cross cut image (a) and (b) are from the CNT forest nanolens, and (c) and (d) are from the PDMS on slits. Each case of CNT forest nanolens and PDMS on slits is simulated using the FDTD method. In (a) and (c), the CNT forest nanolens and PDMS layer are placed at 0-400 nm in the y -axis, respectively. The top views (b) and (d) are taken from 15 nm above the interface of the CNT forest nanolens and PDMS layer. (e) Field intensity passing through the CNT forest nanolens and PDMS slabs are compared. The slit positions are marked with grey bars. The y -axis stands for field intensity and they are in arbitrary units.

In Fig. 4(a), the field distribution of the CNT forest on the double slit is presented. The outgoing electromagnetic fields from the double slit couple to the metallic cylinder array and are carried to the opposite side. While transferring, the electromagnetic fields are carried by surface plasmon polaritons on the metallic cylinder surfaces, so they are spatially confined in the horizontal direction, keeping their high spatial frequencies, which are evanescent. Thus the resolution of the target image (double slit) is determined by the size of the metallic cylinder array. Note that in Fig. 4(b), the brightest speckles are placed at the slit's position. This means that the electromagnetic fields from the double slit have been transferred while keeping their subwavelength scale imaging details.

Figure 4(c) and (d) present the electromagnetic field intensity distributions for the case where the CNT forest was replaced by the PDMS slab. In Fig. 4(c), the electromagnetic field only 100

nm apart from the double slit is blurred. The refractive index of PDMS is 1.4, which is denser than air, so it is deduced that in air, the double slit of 160 nm separation can be resolved only when observation is made within 140 nm away from the slits. Any simple dielectric's (isotropic and homogeneous) refractive index is bigger than that of the air, so a dielectric slab cannot help in resolving the double slit under 532 nm illumination. In contrast, Figs. 3(a), 4(a) and (b) show a clearly resolved double slit image, which has been transferred by the Pt coated CNT forest over a distance of 400 nm. In Fig. 4(e), we plot the averaged electromagnetic field intensities from the cross cut of Fig. 4(b) and (d), and the slit positions together for comparison.

Although the distance 400 nm is shorter than the wavelength (532 nm), the two slits were not resolved over the distance except by the CNTs. If we stack the CNTs array to make the nanolens thicker, as suggested by Kawata *et al.*,¹⁷ the subwavelength scale image could be transferred much further distances. In this regard, our work, demonstrated here, is an important step toward realization of a far-field working nanolens in future.

Conclusions

We have demonstrated a nano-imaging system which can resolve two slits separated by 160 nm with visible light of 532 nm wavelength. That is, the resolving power of the imaging system is at least 0.3 wavelength. The metal coated CNTs, as a wire medium nanolens, successfully transfers nano-scale spatial information from one side to the other side using surface plasmon polariton modes. We made a CNT forest nanolens in the desired shape by controlling the CNT growing conditions. Moreover, the thickness of the nanolens was tailored by microtoming technique. Our work will be helpful in realizing novel optical devices such as a full color supportive far-field nanolens.

Acknowledgements

This research was supported by the Nano R&D Program (No. 2012-0006204) and GNT R&D Program (No. 2012-0006657) through the National Research Foundation of Korea funded by the Ministry of Science, ICT and Future Planning.

Notes and references

^a Creative Research Center for Graphene Electronics, Electronics and Telecommunications Research Institute (ETRI), Daejeon, 305-700,

Republic of Korea. E-mail: cgchoi@etri.re.kr

^b School of Electronics Engineering, Kyungpook National University, Daegu, 702-701, Republic of Korea.

^c Center for Nanomaterials and Chemical Reactions, Institute for Basic Science (IBS), Department of Materials Science and Engineering, Korea Advanced Institute of Science and Technology (KAIST), Daejeon, 305-701, Republic of Korea.

^d Department of Mechanical Engineering, Korea Advanced Institute of Science and Technology (KAIST), Daejeon, 305-701, Republic of Korea.

^e Department of Physics, Korea Advanced Institute of Science and Technology (KAIST), Daejeon, 305-701, Republic of Korea.

1. *Principles of Optics*, 7th ed., M. Born and E. Wolf, Cambridge University Press, Cambridge, 2002.
2. S. Kawata, Y. Inouye, and P. Verma, *Nat. Photonics*, 2009, **3**, 388.
3. C. R. Simovski, P. A. Belov, A. V. Atrashchenko, and Y. S. Kivshar, *Adv. Mater.*, 2012, **24**, 4229.
4. D. Lu and Z. Liu, *Nat. Communications*, 2012, **3**, 1205.

5. S. Kawata, *Jpn. J. Appl. Phys.*, 2013, **52**, 010001.

6. J. B. Pendry, *Phys. Rev. Lett.*, 2000, **85**, 3966.

7. R. A. Shelby, D. R. Smith, and S. Schultz, *Science*, 2001, **292**, 77.

8. C. Luo, S. G. Johnson, and J. D. Joannopoulos, *Phys. Rev. B*, 2002, **65**, 201104.

9. H. J. Lezec, J. A. Dionne, and H. A. Atwater, *Science*, 2007, **316**, 430.

10. A. Mary, S. G. Rodrigo, F. J. Garcia-Vidal, and L. Martin-Moreno, *Phys. Rev. Lett.*, 2008, **101**, 103902.

11. J. Valentine, S. Zhang, T. Zentgraf, E. Ulin-Avila, D. A. Genov, G. Bartal, and X. Zhang, *Nature*, 2008, **455**, 376.

12. N. Fang, H. Lee, C. Sun, and X. Zhang, *Science*, 2005, **308**, 534.

13. Z. Jacob, L. V. Alekseyev, and E. Narimanov, *Opt. Express*, 2006, **14**, 8247.

14. Z. Liu, S. Durant, H. Lee, Y. Pikux, N. Fang, Y. Xiong, C. Sun, and X. Zhang, *Nano Lett.*, 2006, **7**, 403.

15. F. Lemoult, G. Lerosey, J. de Rosny, and M. Fink, *Phys. Rev. Lett.*, 2009, **104**, 203901.

16. J. Rho, Z. Ye, Y. Xiong, X. Yin, Z. Liu, H. Choi, B. Bartal, and X. Zhang, *Nat. Communications*, 2010, **1**, 143.

17. S. Kawata, A. Ono, and P. Verma, *Nat. Photonics*, 2008, **2**, 438.

18. P. A. Belov, G. K. Palikaras, Y. Zhao, A. Rahman, C. R. Simovski, Y. Hao, and C. Parini, *Appl. Phys. Lett.*, 2010, **97**, 191905.

19. B. D. F. Casse, W. T. Lu, Y. J. Huang, E. Gultepe, L. Menon, and S. Sridhar, *Appl. Phys. Lett.*, 2010, **96**, 023114.

20. D. H. Lee, D. O. Shin, W. J. Lee, and S. O. Kim, *Adv. Mater.*, 2008, **20**, 2480.

21. D. H. Lee, W. J. Lee, and S. O. Kim, *Nano Lett.*, 2009, **9**, 1427.

22. Q. Xu, L. Wang, J. Lei, S. Deng, and H. Ju, *J. Mater. Chem. B*, 2013, **1**, 5347.

23. D. H. Lee, J. E. Kim, T. H. Han, J. W. Hwang, S. Jeon, S.-Y. Choi, S. H. Hong, W. J. Lee, R. S. Ruoff, and S. O. Kim, *Adv. Mater.*, 2010, **22**, 1247.

24. *Computational Electrodynamics: The Finite-Difference Time-Domain Method*, 3rd ed., A. Taflov and S. C. Hagness, Artech House, Norwood, 2005.

25. A. Vial and T. Laroche, *J. Phys. D: Appl. Phys.*, 2007, **40**, 7152.

26. *Handbook of Optical Constants of Solids*, E. D. Palik, Academic Press, New York, 1998.